

Controlling the direction of steady electric fields in liquid using nonantiperiodic potentials

Aref Hashemi ^{*}*Courant Institute, New York University, New York, New York 10012, USA*

Mehrdad Tahernia

*Department of Information Engineering, The Chinese University of Hong Kong*William D. Ristenpart [†] and Gregory H. Miller [‡]*Department of Chemical Engineering, University of California Davis, Davis, California 95616, USA*

(Received 22 September 2022; accepted 17 April 2023; published 31 May 2023)

When applying an oscillatory electric potential to an electrolyte solution, it is commonly assumed that the choice of which electrode is grounded or powered does not matter because the time average of the electric potential is zero. Recent theoretical, numerical, and experimental work, however, has established that certain types of multimodal oscillatory potentials that are “nonantiperiodic” can induce a net steady field toward either the grounded or powered electrode [A. Hashemi *et al.*, *Phys. Rev. E* **105**, 065001 (2022)]. Here, we elaborate on the nature of these steady fields through numerical and theoretical analyses of the asymmetric rectified electric field (AREF). We demonstrate that AREFs induced by a nonantiperiodic electric potential, e.g., by a two-mode waveform with modes at 2 and 3 Hz, invariably yields a steady field that is spatially dissymmetric between two parallel electrodes, such that swapping which electrode is powered changes the direction of the field. Furthermore, we show that, while the single-mode AREF occurs in asymmetric electrolytes, nonantiperiodic electric potentials create a steady field in electrolytes even if the cations and anions have the same mobilities. Additionally, using a perturbation expansion, we demonstrate that the dissymmetric AREF occurs due to odd nonlinear orders of the applied potential. We further generalize the theory by demonstrating that the dissymmetric field occurs for all classes of zero-time-average (no dc bias) periodic potentials, including triangular and rectangular pulses, and we discuss how these steady fields can tremendously change the interpretation, design, and applications of electrochemical and electrokinetic systems.

DOI: [10.1103/PhysRevE.107.054608](https://doi.org/10.1103/PhysRevE.107.054608)

I. INTRODUCTION

The application of ac electric potentials to liquids is a ubiquitous element of electrokinetic systems, including induced-charge electrokinetics (ICEK) [1,2], ac electroosmosis (ACEO) [3–6], and electrohydrodynamic (EHD) manipulation of colloids [7–10]. Over the last few decades, a great body of research has focused on evaluating the dynamic response of liquids to ac polarization, in order to find the induced electric field and ion concentrations within the liquid [11–13]. However, ion-containing liquids respond to ac polarizations in intricate ways, especially when the dissolved ions have unequal mobilities. In particular, recent studies have established the existence of an induced, long-range, steady field in liquids, referred to as an asymmetric rectified electric field (AREF) [14–17]. A perfectly sinusoidal potential induces an electric field with a nonzero time average, a zero-frequency component, as a direct result of the nonlinear effects and ionic mobility mismatch. AREF was shown to provide qual-

itative explanations for several long-standing questions in electrokinetics and to significantly change the interpretation of experimental observations [14,18,19].

For a *single-mode* sinusoidal applied potential of amplitude ϕ_0 and angular frequency ω , the one-dimensional AREF between parallel electrodes is antisymmetric with respect to the midplane [14]. Depending on the applied frequency, electrolyte type, and electrode spacing, AREF may change sign several times within the liquid [15]. However, it remains identically zero at the midplane and at the electrodes. Such an antisymmetric shape indicates that the AREF does not change upon swapping the powered and the grounded electrodes, or introducing any time or phase lag to the applied potential.

However, the aforementioned characteristics of AREF do not necessarily hold for other classes of zero-time-average (no dc bias) periodic potentials. In fact, a recent numerical and experimental study by Hashemi *et al.* [20] shows that oscillatory potentials with a certain *time symmetry break* can induce AREFs that are dissymmetric (as different from antisymmetric) in space. Such behavior is reminiscent of so-called “temporal ratchets,” a well-known phenomenon in the context of point particles and optical and quantum lattice systems [21–24]. Here, we provide an extensive numerical and theoretical analysis of the ratchet AREF, its origin, and

^{*}aref@cims.nyu.edu[†]wdristenpart@ucdavis.edu[‡]grgmiller@ucdavis.edu

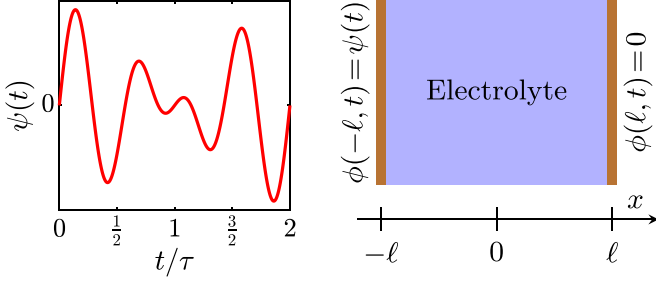


FIG. 1. Schematic diagram of the problem. An electrolyte confined between parallel, planar electrodes, separated by a gap 2ℓ , and powered by a multimodal potential $\psi(t)$ with period 2τ .

its important implications to electrokinetics. In particular, we investigate the AREF induced by an applied multimodal electric potential.

II. PROBLEM STATEMENT

Consider a dilute binary 1-1 electrolyte confined by two parallel, planar electrodes spaced by a gap 2ℓ (Fig. 1). A two-mode potential $\psi(t) = \phi_0[\sin(\omega t) + \sin(\alpha\omega t)]$, with α a rational number, is applied on the electrodes as

$$\phi(-\ell, t) = \psi(t), \quad \phi(\ell, t) = 0. \quad (1)$$

The starting point in theory to investigate the dynamics of such a system is the Poisson-Nernst-Planck (PNP) model. The Poisson equation relates the free charge density to the electric field gradient,

$$-\varepsilon \frac{\partial^2 \phi}{\partial x^2} = \rho = e(n_+ - n_-), \quad (2)$$

while the transport of ions is governed by the Nernst-Planck equations,

$$\frac{\partial n_{\pm}}{\partial t} = D_{\pm} \frac{\partial^2 n_{\pm}}{\partial x^2} \pm \frac{D_{\pm}}{\phi_T} \frac{\partial}{\partial x} \left(n_{\pm} \frac{\partial \phi}{\partial x} \right). \quad (3)$$

Here, the symbols denote permittivity of the electrolyte, ε ; electric potential, ϕ ; free charge number density, ρ ; charge of a proton, e ; thermal potential, ϕ_T ; ion number concentration, n_{\pm} ; diffusivity, D_{\pm} ; location with respect to the midplane, x ; and time, t .

Initially, the ions are uniformly distributed $n_{\pm}(x, 0) = n^{\infty}$ (the bulk electrolyte concentration), and the electric potential is zero everywhere $\phi(x, 0) = 0$. Note that for simplicity, we neglect the intrinsic zeta potential of the electrodes. Finally, at $x = \pm\ell$ (i.e., the electrodes), we set the flux of ions equal to zero (i.e., no electrochemistry).

III. NUMERICAL RESULTS AND DISCUSSION

The system of equations is solved numerically following the algorithm reported by Hashemi *et al.* [14]. (An implementation of this algorithm is freely available online [25].) We focus primarily on the time average of the harmonic solutions defined by

$$\langle \chi \rangle = \frac{1}{2\tau} \int_t^{t+2\tau} \chi dt, \quad 2\tau = \frac{1}{\text{gcd}(1, \alpha)} \frac{2\pi}{\omega}, \quad (4)$$

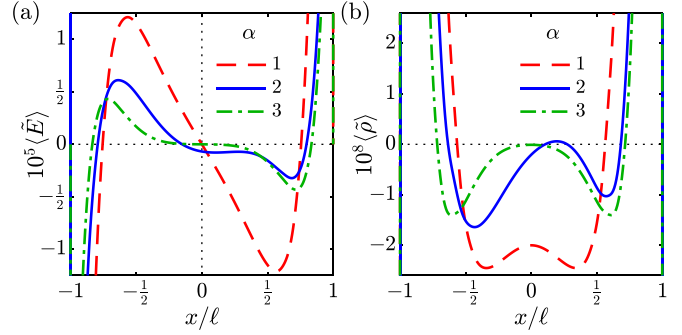


FIG. 2. Representative numerical solutions to (a) the AREF $\langle \vec{E} \rangle = \langle E \rangle / (\kappa \phi_T)$ and (b) time-average free charge density $\langle \bar{\rho} \rangle = \langle \rho \rangle / n^{\infty}$, for two-mode applied potentials $[\phi(t, -\ell) = \phi_0[\sin(\omega t) + \sin(\alpha\omega t)], \phi(t, \ell) = 0]$ in the bulk electrolyte. Parameters: $\phi_0 = 10\phi_T$, $f = \omega/(2\pi) = 50$ Hz, $2\ell = 20$ μm , $D_+ = 10^{-9}$ m^2/s , $D_-/D_+ = 2$, $c^{\infty} = 1$ mM.

where 2τ is the period of the applied potential (or that of the harmonic solution), and $\text{gcd}(1, \alpha)$ is the greatest common divisor of 1 and α [26]. Representative solutions to the AREF (time-average electric field) in the bulk electrolyte (i.e., several Debye layer lengths away from the electrodes) are provided in Fig. 2(a). When $\alpha = 1$, the applied potential is a single-mode sinusoid which yields the antisymmetric AREF [Fig. 2(a), dashed red curve]. The case of $\alpha = 2$ reveals a surprising phenomena: the shape of the AREF becomes dissymmetric with a nonzero value even at the midplane [Fig. 2(a), solid blue curve]. Further complicating matters, for $\alpha = 3$, the AREF is again perfectly antisymmetric [Fig. 2(a), dashed-dotted green curve]. Therefore, it appears that depending on α , the induced AREF can be either antisymmetric with a zero value at the midplane or dissymmetric. The corresponding spatial distributions of the time-average free charge density $\langle \rho \rangle$ are illustrated in Fig. 2(b) for different α values. Consistent with the AREF distributions in Fig. 2(a), $\langle \rho \rangle$ is spatially even for $\alpha = 1$ and 3, but takes a dissymmetric shape for $\alpha = 2$.

The behavior becomes more complicated at the Debye scale (i.e., up a few Debye lengths away from the electrodes). Figures 3(a) and 3(b) show the AREF within 4 Debye lengths away from the electrodes for $\alpha = 1$ and 2. When $\alpha = 1$ (i.e., a single-mode sinusoidal potential), AREF is zero at the electrodes, which is a direct result of the antisymmetric shape of the AREF and the total charge neutrality. The former can be clarified by a parity analysis of the second-order perturbation solution (in terms of the applied potential) to the problem (see Supplemental Material [27]). The total charge neutrality on the other hand enforces the AREF at one electrode to be equal to that on the other electrode, that is $\langle E \rangle_{-\ell} = \langle E \rangle_{\ell} = K$ for some constant K . But, for AREF to be antisymmetric, K has to be zero. It is worth mentioning that while the total charge neutrality is held (and enforced by the boundary conditions), AREF breaks the *local* charge neutrality. It can be seen from the nonuniform spatial structure of the AREF and a consideration of Gauss's law.

When $\alpha = 2$, an astonishingly large AREF is induced on the electrodes (≈ 4 orders of magnitude larger than the AREF in the bulk electrolyte). We note, however, that the

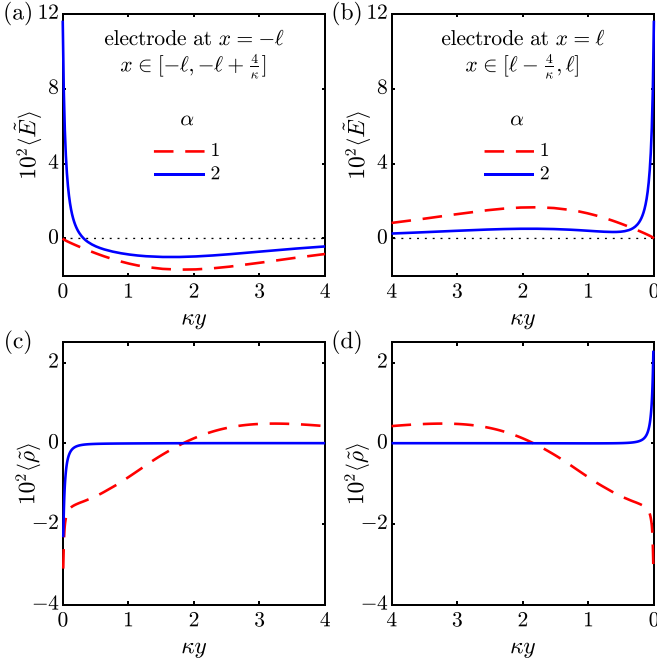


FIG. 3. Representative numerical solutions to (a), (b) the AREF $\langle \vec{E} \rangle = \langle E \rangle / (\kappa \phi_T)$ and (c), (d) time-average free charge density $\langle \bar{\rho} \rangle = \langle \rho \rangle / n^\infty$, for two-mode applied potentials $[\phi(t, -\ell) = \phi_0[\sin(\omega t) + \sin(\alpha \omega t)], \phi(t, \ell) = 0]$ at the Debye scale. For visualization purposes, the $\langle \bar{\rho} \rangle$ data for $\alpha = 2$ in (c) and (d) are divided by 100. The spatial variable y denotes the distance from the corresponding electrode. Parameters: $\phi_0 = 10\phi_T$, $f = \omega/(2\pi) = 50$ Hz, $2\ell = 20$ μm , $D_+ = 10^{-9}$ m^2/s , $D_-/D_+ = 2$, $c^\infty = 1$ mM.

total charge neutrality still holds. The mere observation of a nonzero AREF at the electrodes for $\alpha = 2$ is consistent with the dissymmetric shape of AREF in the bulk electrolyte: The integral of the AREF over the entire domain has to be zero, i.e., $\int_{-\ell}^{\ell} \langle E \rangle dx = \langle \phi \rangle_{-\ell} - \langle \phi \rangle_{\ell} = 0$. In other words, the nonzero AREF at the electrodes and the dissymmetric shape of the AREF in the bulk electrolyte are interrelated. A qualitatively consistent behavior is observed for the distribution of ρ [Figs. 3(c) and 3(d)]. The induced $\langle \rho \rangle$ on the two electrodes are the same for $\alpha = 1$. However, when $\alpha = 2$, there is a sign flip in the time-average free charge density induced at the two electrodes ($\langle \rho \rangle_{-\ell} = -\langle \rho \rangle_{\ell}$).

We now ask what happens if we flip the sign of the applied potential $[-\psi(t)$ instead of $\psi(t)]$. For $\alpha = 1$ (antisymmetric AREF), the curves of the induced AREF by $\psi(t)$ and $-\psi(t)$ potentials are superimposed [Fig. 4(a)]. However, flipping the sign of the potential when $\alpha = 2$ (dissymmetric AREF) yields a mirrored version of the AREF with respect to the midplane [Fig. 4(b)]. It is worth mentioning that the sum of the solid red $[\psi(t)]$ and dashed blue $[-\psi(t)]$ curves in Fig. 4(b) is antisymmetric and zero at the midplane; the dissymmetric components of the AREFs due to $\psi(t)$ and $-\psi(t)$ potentials cancel each other.

We provide an explanation for this numerical observation using symmetry arguments. Note that the field-induced ion motion depends only on the potential gradient (not the potential itself). Therefore, one can show that flipping the sign of a periodic, time-varying potential $\psi(t)$ at $x = -\ell$ is equivalent

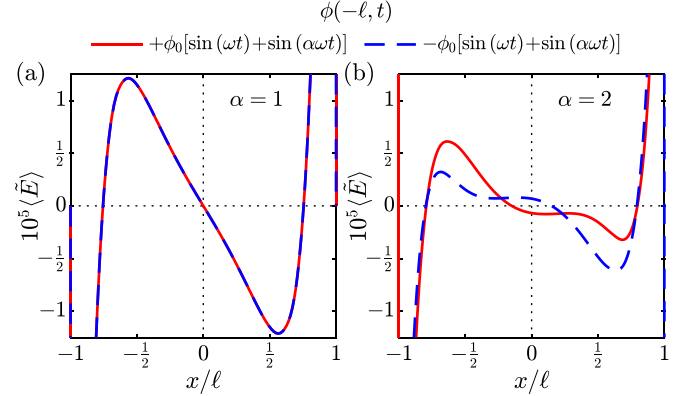


FIG. 4. Flipping the sign of the applied potential at $x = -\ell$ for (a) $\alpha = 1$ and (b) $\alpha = 2$. Parameters: $\phi_0 = 10\phi_T$, $f = \omega/(2\pi) = 50$ Hz, $2\ell = 20$ μm , $D_+ = 10^{-9}$ m^2/s , $D_-/D_+ = 2$, $c^\infty = 1$ mM.

to swapping the powered and grounded electrodes [by adding the potential $\psi(t)$ to the both electrodes]. In other words, the electric field induced by applying $-\psi(t)$ on the electrode at $x = -\ell$ is the same as that induced by applying $\psi(t)$ on the electrode at $x = \ell$. Now, a simple change of variable $x \rightarrow -x$ clarifies that if the potential $\psi(t)$ yields the electric field $E(x, t)$, the potential $-\psi(t)$ would yield the mirrored version, $-E(-x, t)$ [cf. Fig. 4(b)].

Focusing on the midplane ($x = 0$), one can write that the functional $E(0, t) = \epsilon(t) = f(\psi, t)$ is odd in ψ . Therefore, if $\epsilon(t)$ is the induced electric field at the midplane due to the potential $\psi(t)$, $-\epsilon(t)$ would be that due to the potential $-\psi(t)$. Now consider antiperiodic potentials, i.e., $\psi(t + \tau) = -\psi(t)$. We prove that $\langle \epsilon \rangle$ (i.e., AREF at the midplane) has to be zero for antiperiodic potentials:

$$\epsilon(t + \tau) = f(\psi, t + \tau) = f(-\psi, t) = -\epsilon(t). \quad (5)$$

Therefore, $\epsilon(t + \tau) = -\epsilon(t)$, which upon taking a time average yields $\langle \epsilon \rangle = -\langle \epsilon \rangle$, indicating $\langle \epsilon \rangle = 0$. It is worth mentioning that the above argument is general and holds for any antiperiodic potential $\psi(t)$. It appears that for such potentials the zero-frequency components of the induced electric field cancel each other at the midplane, yielding an antisymmetric AREF. However, they do not necessarily cancel out when the excitation is nonantiperiodic.

Figure 5 illustrates several examples of the antiperiodic and nonantiperiodic two-mode potentials. One can show that $\psi(t)$ is antiperiodic if α , in its simplified fractional form, can be expressed as {odd integer}/{odd integer} (e.g., $\alpha = 1, \frac{5}{3}, 3, 5, \dots$). Otherwise, the two-mode potential is nonantiperiodic (e.g., $\alpha = 2, \frac{4}{3}, \frac{3}{2}, 4, \dots$). (See Hashemi *et al.* [20] for a simple proof.) Our numerical results for a wide range of α values corroborate our theory. For all antiperiodic potentials tested, the AREF is zero at the midplane, and is antisymmetric in space [e.g., $\alpha = 1$ and 3 in Fig. 2(a)]. Furthermore, a dissymmetric AREF with a nonzero value at the midplane is induced for nonantiperiodic potentials [e.g., $\alpha = 2$ in Fig. 2(a)]. It should be noted though that the degree by which the AREF becomes dissymmetric is a complicated function of α . However, regardless of the system parameters,

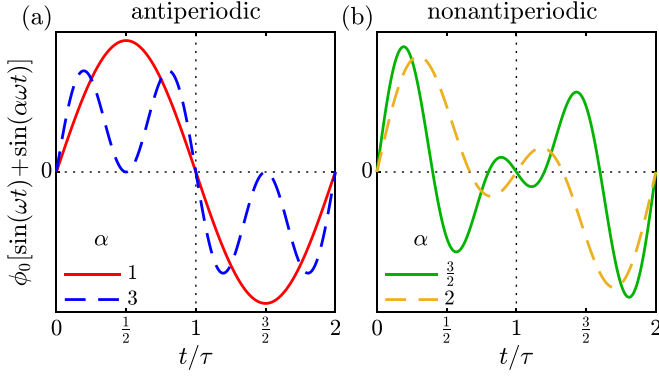


FIG. 5. Examples of (a) antiperiodic and (b) nonantiperiodic two-mode applied potentials $\phi_0[\sin(\omega t) + \sin(\alpha\omega t)]$.

$\alpha = 2$ appears to induce the most significant dissymmetric behavior.

In Fig. 6(a), we show the effect of the two-mode potential amplitude ϕ_0 on the induced AREF for $\alpha = 2$. As a high-order nonlinear phenomenon [34], the dissymmetry rapidly grows with the amplitude. At sufficiently low amplitudes, the dissymmetry disappears and the AREF is almost antisymmetric [cf. Fig. 6(a), dashed red curve]. An interesting finding here is that unlike the single-mode AREF, the curves of different voltage amplitudes do not collapse. There is no scaling factor (as a function of Φ_0) that maps all of the AREF curves onto a master curve. This is particularly significant to the application of the AREF in particle height bifurcation [35,36]. It has been established that for a single-mode potential, the AREF-induced levitation height of charged colloids is insensitive to the amplitude of the potential, as are the zeros of the AREF, which determine approximately the heights at which the total force on a colloid is zero [14,18]. Here, however, the zeros of the AREF, and hence the levitation heights of the colloids, depend on the applied potential. This adds another parameter, along with the applied frequency, to tune the levitation height.

The effect of the applied frequency $f = \omega/(2\pi)$ is more complicated. Even for a single-mode potential, it has been established that the spatial oscillation of the AREF (its shape) is very sensitive to frequency [14,15]. For the two-mode po-

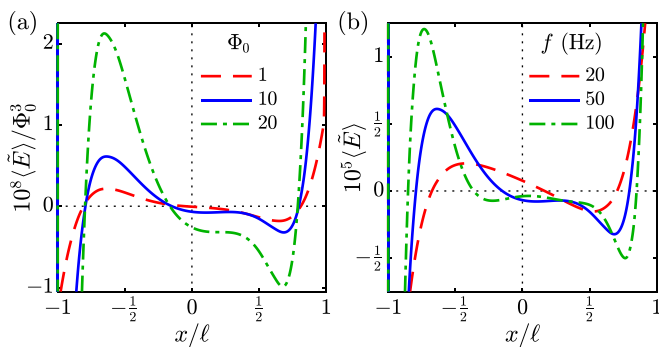


FIG. 6. Effects of the (a) two-mode potential amplitude and (b) frequency on the dissymmetric AREF. For visualization purposes the data in (a) are scaled by Φ_0^3 with $\Phi_0 = \phi_0/\phi_T$. Parameters: $\phi_0 = 10\phi_T$ for (b), $f = \omega/(2\pi) = 50$ Hz for (a), $\alpha = 2$, $2\ell = 20 \mu\text{m}$, $D_+ = 10^{-9} \text{m}^2/\text{s}$, $D_-/D_+ = 2$, $c^\infty = 1 \text{mM}$.

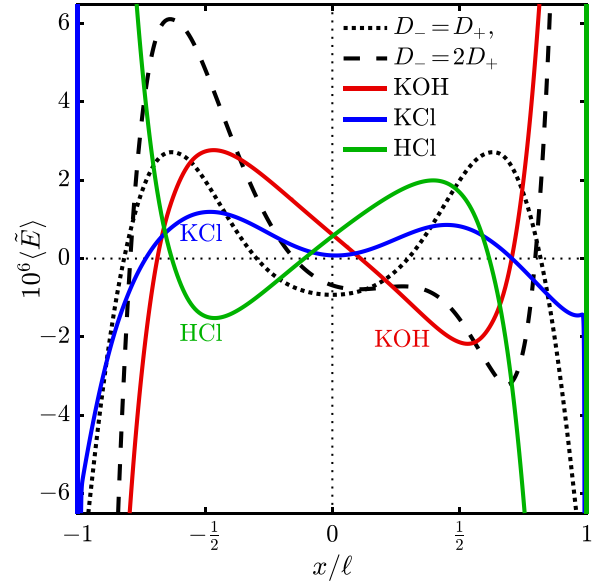


FIG. 7. Spatial structure of the dissymmetric AREF for different 1-1 binary electrolytes. Parameters: $\phi_0 = 10\phi_T$ for (b), $f = \omega/(2\pi) = 50$ Hz for (a), $\alpha = 2$, $2\ell = 20 \mu\text{m}$, $c^\infty = 1 \text{mM}$. The reference results correspond to $D_+ = 10^{-9} \text{m}^2/\text{s}$.

tential, similar to the antisymmetric AREF, increasing the frequency amplifies the AREF peak magnitude in the bulk and shifts the peak location toward the electrodes [14,15], albeit through a more complex pattern [cf. Fig. 6(b)]. Furthermore, we note that the dissymmetry intensifies substantially with frequency. More importantly, the sign of AREF at the mid-plane is changed upon changing the frequency.

In Fig. 7 we inspect the effect of electrolyte type on the dissymmetric AREF. We focus here only on 1-1 electrolytes, and defer an analysis of electrolytes with valence mismatch to future efforts. Two reference results for $D_-/D_+ = 1$ and 2 are also depicted for comparison. We observe that changing the electrolyte from KOH ($D_+ = 1.96 \times 10^{-9} \text{m}^2/\text{s}$, $D_- = 5.27 \times 10^{-9} \text{m}^2/\text{s}$) to HCl ($D_+ = 9.31 \times 10^{-9} \text{m}^2/\text{s}$, $D_- = 2.03 \times 10^{-9} \text{m}^2/\text{s}$) reverses the direction of the dissymmetric AREF. Such a field reversal has been observed for the single-mode AREF as well (see for example Fig. 2 in Ref. [14] and Fig. 8 in Ref. [16]). Interestingly, for KCl, with $D_+ \approx D_-$ ($D_+ = 1.96 \times 10^{-9} \text{m}^2/\text{s}$, $D_- = 2.03 \times 10^{-9} \text{m}^2/\text{s}$), we observe a steady field with magnitudes comparable to KOH and HCl, which is unexpected for such a moderate amplitude of the electric potential. (See Ref. [15] for a detailed analysis of the effect of ionic mobility mismatch on the magnitude of the AREF.) In fact, our results indicate that the steady field is generated even in a symmetric electrolyte (see the $D_+ = D_-$ case in Fig. 7). In contrast, the single-mode AREF can only be generated in asymmetric electrolytes. Here, the source of asymmetry that yields the steady field is the applied nonantiperiodic electric potential.

Following Hashemi *et al.* [14], we have performed several consistency checks on the numerical results, such as the feasibility of the calculated instantaneous ion concentrations, electric field, and induced zeta potential at the electrode surface. Furthermore, the numerical solution converges and

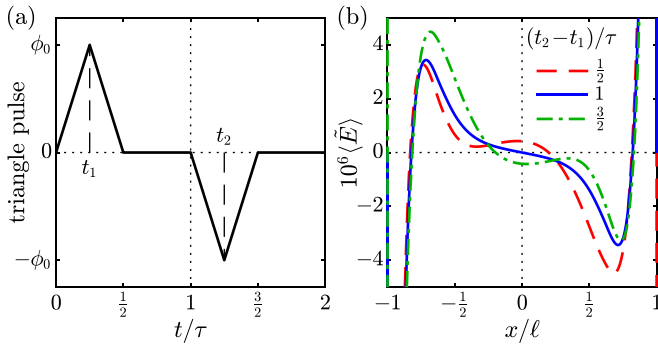


FIG. 8. Dissymmetric AREF due to a zero-time-average triangular pulse potential applied at $x = -\ell$. (a) Positive (at $t = t_1$) and negative (at $t = t_2$) triangular pulses of width $\frac{1}{2}\tau$ and amplitude ϕ_0 . (b) The corresponding induced AREF for different values of $(t_2 - t_1)/\tau$. Parameters: $\phi_0 = 20\phi_T$, $1/(2\tau) = 50$ Hz, $2\ell = 20$ μm , $D_+ = 10^{-9}$ m^2/s , $D_-/D_+ = 2$, $c^\infty = 1$ mM.

the total mass is conserved. We have inspected the total charge neutrality by $\int_{-\ell}^{\ell} \partial^2 \langle \phi \rangle / \partial x^2 dx = 0$ and, alternatively, by $\langle E \rangle_{-ell} = \langle E \rangle_{ell}$. The condition $\int_{-\ell}^{\ell} \langle E \rangle = 0$ is also checked to ensure that the numerical solution satisfies the boundary conditions. A concern in the dynamic solution of the PNP equations under oscillatory polarization is whether quasi-steady-state conditions (harmonic solution) are achieved. We have accurately checked that the quasisteady conditions are attained for the present numerical results.

We emphasize that our theory is not limited to any specific potential waveform. A general zero-mean function $\psi(t)$ with a period 2τ has a Fourier series of the form $\psi(t) = \sum_{n=1}^{\infty} [a_n \cos(n\pi t/\tau) + b_n \sin(n\pi t/\tau)]$, which is antiperiodic if $a_n = b_n = 0$ for even n . Therefore, any antiperiodic $\psi(t)$ can be expressed as

$$\psi(t) = \sum_{n=1,3,\dots}^{\infty} \left[a_n \cos\left(\frac{n\pi t}{\tau}\right) + b_n \sin\left(\frac{n\pi t}{\tau}\right) \right], \quad (6)$$

and the ratio of any two frequencies will be the ratio of two odd integers.

It should be understood that for a given applied potential $\psi(t)$ in the first half of the period $t \in [0, \tau]$, there is a unique antiperiodic potential that occurs by setting $\psi(t + \tau) = -\psi(t)$. But an infinite number of nonantiperiodic potentials can be constructed. We demonstrate this argument

for a triangular pulse of period 2τ , illustrated in Fig. 8. Two pulses of amplitude ϕ_0 and width $\frac{1}{2}\tau$ are applied at $t_1 = \frac{1}{4}\tau$ and $\frac{3}{4}\tau \leq t_2 \leq \frac{7}{4}\tau$. We keep t_1 fixed and vary t_2 to cover all possible cases. The induced AREFs are shown in Fig. 8(b) for different $t_2 - t_1$ values. The AREF is antisymmetric only if $t_2 - t_1 = \tau$ for which the potential in the second half period becomes the negative of that in the first half [Fig. 8(b), solid blue curve]. All other constructions yield a dissymmetric AREF. It is interesting to note that the cases $t_2 - t_1 = \frac{1}{2}\tau$ (consecutive pulses in the first half) and $t_2 - t_1 = \frac{3}{2}\tau$ (maximally apart pulses) provide the maximum dissymmetry and are mirrored. A simple time shift $t \rightarrow \frac{3}{2}\tau$ shows that the condition of maximally apart pulses is actually the negative version of the back-to-back pulses, and therefore yields the mirrored version of the AREF [cf. Fig. 4(b)].

IV. CONCLUSIONS

In summary, our results show that ions and charged colloids can be concentrated to one side of a slit channel, or another, by tuning the applied potential waveform. We demonstrate that the induced AREF between parallel electrodes by a nonantiperiodic electric potential is spatially dissymmetric. An intriguing implication is then that swapping the powered and grounded electrodes of an electrochemical cell alters the system behavior, an observation at odds with the classical understanding of the electrokinetics. The dissymmetric AREF can tremendously change the design of electrokinetic systems and their applications. It was recently shown at length that the AREF-induced electrophoretic forces are several orders of magnitude larger than gravitational and colloidal forces [14,15,18,19]. Researchers can therefore use the dissymmetric AREF to design electrochemical cells that selectively (to some extent) separate charged colloidal particles or bioparticles near the powered or the grounded electrodes. Moreover, the sole physical implications of the dissymmetric AREF opens another chapter for the researchers in the electrokinetic community.

ACKNOWLEDGMENT

This material is based upon work partially supported by the National Science Foundation under Grants No. DMS-1664679 and No. CBET-2125806.

[1] M. Z. Bazant and T. M. Squires, *Phys. Rev. Lett.* **92**, 066101 (2004).
 [2] T. M. Squires and M. Z. Bazant, *J. Fluid Mech.* **509**, 217 (1999).
 [3] A. Ramos, H. Morgan, N. G. Green, and A. Castellanos, *J. Phys. D: Appl. Phys.* **31**, 2338 (1998).
 [4] A. Ramos, H. Morgan, N. G. Green, and A. Castellanos, *J. Colloid Interface Sci.* **217**, 420 (1999).
 [5] A. Ajdari, *Phys. Rev. E* **61**, R45(R) (2000).
 [6] V. Studer, A. Pepin, Y. Chen, and A. Ajdari, *Analyst* **129**, 944 (2004).

[7] M. Trau, D. A. Saville, and I. Aksay, *Science* **272**, 706 (1996).
 [8] D. C. Prieve, P. J. Sides, and C. L. Wirth, *Curr. Opin. Colloid Interface Sci.* **15**, 160 (2010).
 [9] F. Ma, S. Wang, L. Smith, and N. Wu, *Adv. Funct. Mater.* **22**, 4334 (2012).
 [10] C. S. Dutcher, T. J. Woehl, N. H. Talken, and W. D. Ristenpart, *Phys. Rev. Lett.* **111**, 128302 (2013).
 [11] M. Z. Bazant, K. Thornton, and A. Ajdari, *Phys. Rev. E* **70**, 021506 (2004).
 [12] M. Z. Bazant, M. S. Kilic, B. D. Storey, and A. Ajdari, *Adv. Colloid Interface Sci.* **152**, 48 (2009).

- [13] A. Ramos, P. Garcia-Sanchez, and H. Morgan, *Curr. Opin. Colloid Interface Sci.* **24**, 79 (2016).
- [14] A. Hashemi, S. C. Bukosky, S. P. Rader, W. D. Ristenpart, and G. H. Miller, *Phys. Rev. Lett.* **121**, 185504 (2018).
- [15] A. Hashemi, G. H. Miller, and W. D. Ristenpart, *Phys. Rev. E* **99**, 062603 (2019).
- [16] A. Hashemi, G. H. Miller, K. J. M. Bishop, and W. D. Ristenpart, *Soft Matter* **16**, 7052 (2020).
- [17] B. Balu and A. S. Khair, *J. Eng. Math.* **129**, 4 (2021).
- [18] S. C. Bukosky, A. Hashemi, S. P. Rader, J. Mora, G. H. Miller, and W. D. Ristenpart, *Langmuir* **35**, 6971 (2019).
- [19] A. Hashemi, G. H. Miller, and W. D. Ristenpart, *Phys. Rev. Fluids* **5**, 013702 (2020).
- [20] A. Hashemi, M. Tahernia, T. C. Hui, W. D. Ristenpart, and G. H. Miller, *Phys. Rev. E* **105**, 065001 (2022).
- [21] S. Flach, O. Yevtushenko, and Y. Zolotaryuk, *Phys. Rev. Lett.* **84**, 2358 (2000).
- [22] S. Denisov, S. Flach, A. A. Ovchinnikov, O. Yevtushenko, and Y. Zolotaryuk, *Phys. Rev. E* **66**, 041104 (2002).
- [23] A. V. Ustinov, C. Coqui, A. Kemp, Y. Zolotaryuk, and M. Salerno, *Phys. Rev. Lett.* **93**, 087001 (2004).
- [24] S. Denisov, S. Flach, and P. Hanggi, *Phys. Rep.* **538**, 77 (2014).
- [25] <https://github.com/rfjd/1D-PNP-Numerical-Solution>.
- [26] For two rational numbers a_1 and a_2 , $\gcd(a_1, a_2)$ can be computed by $\gcd(N_1, N_2)/\text{lcm}(D_1, D_2)$, where $N_{1,2}$ and $D_{1,2}$ are, respectively, the integer numerators and denominators of $a_{1,2}$ written as fractions (both reduced), and lcm denotes the least common multiple operator.
- [27] See Supplemental Material at <http://link.aps.org/supplemental/10.1103/PhysRevE.107.054608> for a detailed perturbation analysis of the problem, which includes Refs. [16,28–33].
- [28] E. H. B. Delacey and L. R. White, *J. Chem. Soc., Faraday Trans. 2* **77**, 2007 (1981).
- [29] C. S. Mangelsdorf and L. R. White, *J. Chem. Soc., Faraday Trans. 88*, 3567 (1992).
- [30] C. S. Mangelsdorf and L. R. White, *J. Chem. Soc., Faraday Trans. 93*, 3145 (1997).
- [31] E. J. Hinch, J. D. Sherwood, W. C. Chew, and P. N. Sen, *J. Chem. Soc., Faraday Trans. 2* **80**, 535 (1984).
- [32] I. Lelidis and G. Barbero, *Phys. Lett. A* **343**, 440 (2005).
- [33] G. Barbero and I. Lelidis, *Phys. Rev. E* **76**, 051501 (2007).
- [34] Using a perturbation analysis after Ref. [16], the dissymmetric behavior of the $\alpha = 2$ case can be shown by a third-order expansion. We suspect, but have not proven, that other dissymmetric cases can be shown with higher-order perturbation expansions (see Supplemental Material [27]).
- [35] T. J. Woehl, B. J. Chen, K. L. Heatley, N. H. Talken, S. C. Bukosky, C. S. Dutcher, and W. D. Ristenpart, *Phys. Rev. X* **5**, 011023 (2015).
- [36] S. C. Bukosky and W. D. Ristenpart, *Langmuir* **31**, 9742 (2015).